

Nonlinear quantum dynamics in a \mathcal{PT} -symmetric double well

Daniel Haag,* Dennis Dast, Andreas Löhle, Holger Cartarius, Jörg Main, and Günter Wunner
Institut für Theoretische Physik 1, Universität Stuttgart, 70550 Stuttgart, Germany

(Dated: July 19, 2018)

We investigate the mean-field dynamics of a Bose-Einstein condensate (BEC) described by the Gross-Pitaevskii equation (GPE) in a double-well potential with particle gain and loss, rendering the system \mathcal{PT} -symmetric. The stationary solutions of the system show a change from elliptically stable behavior to hyperbolically unstable behavior caused by the appearance of \mathcal{PT} -broken solutions of the GPE and influenced by the nonlinear interaction. The dynamical behavior is visualized using the Bloch sphere formalism. However, the dynamics is not restricted to the surface of the sphere due to the nonlinear and non-Hermitian nature of the system.

PACS numbers: 03.75.Kk, 11.30.Er, 03.65.Ge

I. INTRODUCTION

The interaction with the environment often plays an important role in studies of ultracold atoms, leading to gain or loss of particles. One important example is the inelastic three-body collision of particles in a BEC which can be described in mean-field approximation by an imaginary interaction potential, thus rendering the Hamiltonian non-Hermitian [1, 2]. Imaginary potentials also find application in studies of dissipative optical lattices [3, 4], and the non-Hermitian GPE has been derived as the mean-field limit of an open Bose-Hubbard system described by a master equation in Lindblad form [5, 6]. A gain of particles is less described in literature, but the feeding of a condensate from a thermal cloud has been described by a positive imaginary potential [2].

We study the dynamics of a BEC in a double-well potential where particles are coherently removed from one well and injected into the other. The system is described in mean-field approximation by the GPE. The GPE is known to yield accurate results for temperatures considerably smaller than the critical temperature of the condensate but has limitations in the vicinity of dynamic instabilities [7, 8]. The removal and injection of particles is described by an imaginary potential. Both a coherent influx and outflux have been experimentally realized. A coherent particle loss has, e.g., been implemented using a focused electron beam [9] whereas the influx can be provided from a second condensate exploiting electronic excitations of the atoms [10].

The gain and loss contributions are chosen in such a way that the resulting system is \mathcal{PT} -symmetric, where \mathcal{P} denotes the parity operator $\hat{x} \rightarrow -\hat{x}$, $\hat{p} \rightarrow -\hat{p}$ and \mathcal{T} the time reversal operator $\hat{p} \rightarrow -\hat{p}$, $i \rightarrow -i$. Even though being non-Hermitian, such systems can exhibit entirely real eigenvalues in certain parameter regimes [11]. In recent years efforts have been pursued to establish a quantum theory in which the requirement of Hermiticity is replaced by the weaker condition of

\mathcal{PT} symmetry [12, 13] or by the more general concept of pseudo-Hermiticity [14–16]. Besides these fundamental approaches to generalize quantum mechanics a great variety of \mathcal{PT} -symmetric systems which are potentially experimentally accessible has been theoretically investigated [17–22]. The experimental breakthrough succeeded in optical waveguide systems [17, 23, 24], now being one of the main foci in the field of \mathcal{PT} symmetry.

For the system considered \mathcal{PT} symmetry demands that the influx and outflux of particles into or from the condensate is balanced in such a way that stationary solutions can be found. Embedding the \mathcal{PT} -symmetric double well into a Hermitian four-well potential is a possible experimental realization of this system [25].

Prior to the experimental realization of a \mathcal{PT} -symmetric nonlinear quantum system it is of utmost importance to have a detailed understanding of the dynamical behavior resulting from the combination of \mathcal{PT} symmetry and nonlinearity. In particular it is necessary to study the implications on the stability properties of the stationary solutions since only stable states are observable. However, not only the stability of stationary states but also the dynamics of arbitrary wave packets is relevant because for certain initial wave packets the number of particles diverges, thus destroying the condensate. We will address these problems, laying the foundation for future attempts of an experimental realization of a \mathcal{PT} -symmetric Bose-Einstein condensate.

In this article we solve the dimensionless GPE with contact interaction

$$[-\Delta + V(\mathbf{r}) + 8\pi N_0 a |\psi(\mathbf{r}, t)|^2] \psi(\mathbf{r}, t) = i \frac{\partial}{\partial t} \psi(\mathbf{r}, t), \quad (1)$$

where N_0 is the number of particles and a is the scattering length. The three-dimensional double-well potential chosen,

$$V(\mathbf{r}) = \frac{1}{4}x^2 + \frac{1}{4}\omega_{y,z}^2(y^2 + z^2) + v_0 e^{-\sigma x^2} + i\gamma x e^{-\rho x^2}, \quad (2)$$

is \mathcal{PT} -symmetric since $V(\mathbf{r}) = V^*(-\mathbf{r})$ holds. The potential consists of a three-dimensional harmonic trap with an identical trapping frequency $\omega_{y,z}$ in y and z direction. The harmonic trap in x direction is superimposed

* Daniel.Haag@itp1.uni-stuttgart.de

by a Gaussian barrier with height v_0 and width parameter σ , thus forming a symmetric double-well potential. The strength of the antisymmetric imaginary part of the potential is tuned by γ , and the parameter ρ is chosen in such a way that the extrema of the imaginary part coincide with the minima of the double well. The positive imaginary part can be interpreted as a source of probability density while a negative part corresponds to a sink. In all following calculations the values $\omega_{y,z} = 2$, $v_0 = 4$, $\sigma = 0.5$, and $\rho \approx 0.12$ are fixed whereas the gain/loss parameter γ and the strength of the nonlinearity N_0a are varied.

Since the system is non-Hermitian the norm of the wave function ψ is not conserved and due to the nonlinearity of the GPE a different norm changes the dynamics. The physical interpretation of a change in the norm of the wave function is a change in the number of particles

$$N = N_0 \|\psi\|^2. \quad (3)$$

Without interaction, i.e. $Na = 0$, the Hamiltonian is separable and is solved by the product ansatz $\psi(x)\psi_m(y)\psi_m(z)$, where ψ_m is the m -th eigenstate of the one-dimensional harmonic oscillator. Since the energy of the first excited state of the harmonic oscillator is about one order of magnitude larger than that of the first excited state of the double well, only the ground states of the harmonic oscillators in y and z direction are taken into account. Thus the three-dimensional problem is reduced to one dimension with the one-dimensional \mathcal{PT} -symmetric double-well potential

$$V(x) = \frac{1}{4}x^2 + v_0e^{-\sigma x^2} + i\gamma x e^{-\rho x^2}. \quad (4)$$

This can easily be solved by a numerically exact integration. The product ansatz does not exactly solve the nonlinear GPE with contact interaction, however, for small values of Na it is still a good approximation, and as we will see not only shows qualitatively the same behavior as the calculations in three dimensions but also quantitatively.

The article is organized as follows. In Sec. II the stationary solutions in three dimensions are presented and a comparison with the one-dimensional solutions is drawn. To study the stability of the stationary solutions the Bogoliubov-de Gennes equations are adapted for non-Hermitian systems and solved numerically in Sec. III. In Sec. IV the time evolution of wave packets is investigated using the Bloch sphere formalism. Conclusions are drawn in Sec. V.

II. STATIONARY SOLUTIONS

The eigenvalue spectrum and eigenstates of a BEC in the \mathcal{PT} -symmetric double well (4) have already been discussed [26, 27], however, only as a function of the

gain/loss parameter γ . To study dynamical properties it is more instructive to discuss the eigenvalues as a function of Na , where N is the effective number of particles as defined in Eq. (3).

To solve the three-dimensional system we use the *time-dependent variational principle* [28–31] whose application to \mathcal{PT} -symmetric nonlinear systems has been discussed in [26]. Our ansatz consists of coupled Gaussian functions

$$\psi(\mathbf{r}) = \sum_{\mathbf{k}} \exp \left[-A_x^{\mathbf{k}}(x - q_x^{\mathbf{k}})^2 + A_{y,z}^{\mathbf{k}}(y^2 + z^2) - ip_x^{\mathbf{k}}(x - q_x^{\mathbf{k}}) + \varphi^{\mathbf{k}} \right] \quad (5)$$

with $A_x^{\mathbf{k}}, A_{y,z}^{\mathbf{k}}, \varphi^{\mathbf{k}} \in \mathbb{C}$, $q_x^{\mathbf{k}}, p_x^{\mathbf{k}} \in \mathbb{R}$. The variational principle yields equations of motion for these time-dependent quantities, and stationary solutions are found as the fixed points of these equations. The stationary solutions of the three-dimensional potential (2) presented in this section are gained with the variational approach whereas the one-dimensional potential (4) is solved numerically exact. We use up to two Gaussian functions per well, i.e. up to four Gaussians in total, which yields a small correction to one Gaussian function per well.

A. Spectrum of the real double well

Figure 1 shows the eigenvalues of the GPE in the three-dimensional \mathcal{PT} -symmetric double well (2) with the lowest total energy. For $\gamma = 0$ the spectrum in Fig. 1(a) contains three pairs of states each of which form a common branch, shown as blue solid, yellow dashed and green dot-dashed lines. Note that the blue and yellow branches almost lie on top of each other. Every branch is born in a tangent bifurcation at a critical value of Na . At the three tangent bifurcations not only the eigenvalues but also the eigenstates coincide.

The two bifurcations for the blue and yellow branches reside at almost identical values $Na \approx -1.4$. The states arising at these tangent bifurcations have an equal probability of presence in both wells. At one bifurcation two states with symmetric (even parity) wave functions arise (blue solid lines), whereas the two states arising at the other bifurcation (yellow dashed lines) are antisymmetric (odd parity). At the bifurcation points the wave functions turn into two peaks strongly confined in the two wells due to the attractive interaction. For stronger attractive interactions no stationary solutions exist and the condensate collapses [32, 33].

The same collapse is observed at approximately half the interaction strength $Na \approx -0.7$ (green dot-dashed branch) where the wave function is entirely localized in one well, i.e. it corresponds to exactly the same collapse process of the wave function, but for an asymmetric wave restricted to one side of the double well. The states arising at this bifurcation are clearly parity symmetry broken and doubly degenerate because the condensate can be located either in the right or in the left well. The

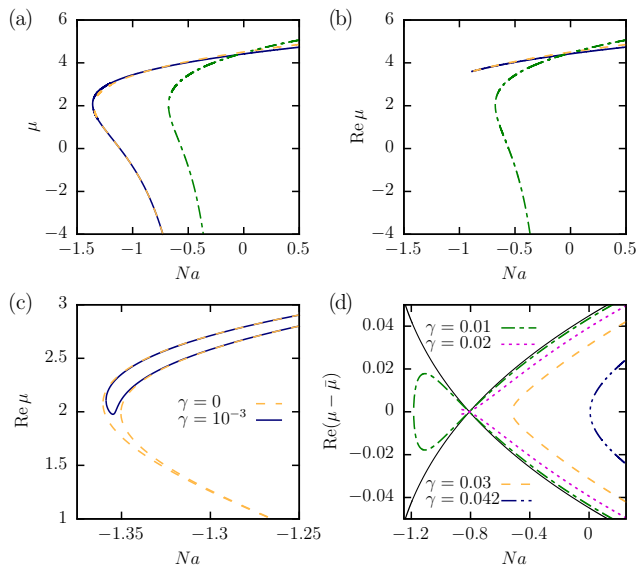


Figure 1. (Color online) (a) The chemical potential μ of the eigenvalues without gain/loss, i.e. $\gamma = 0$, as a function of the particle number scaled scattering length. The symmetric (blue solid branch) and antisymmetric (yellow dashed branch) stationary solutions arise at two almost identical bifurcation points at $Na \approx -1.4$, and the doubly degenerate symmetry-breaking eigenstates (green dot-dashed branch) at $Na \approx -0.7$. (b) Introducing the gain/loss $\gamma = 0.02$ hardly changes $\text{Re } \mu$ of the symmetry-breaking (\mathcal{PT} -broken) eigenstates but the two \mathcal{PT} -symmetric branches now arise at a tangent bifurcation. (c) The tangent bifurcation of the two \mathcal{PT} -symmetric states in the vicinity of the bifurcation point for a small value of γ . (d) The difference between the chemical potential of the \mathcal{PT} -symmetric states and their mean value $\bar{\mu}$. Different values of γ are compared to the case $\gamma = 0$ (black solid line).

two uppermost panels of Fig. 2 shows the eigenvalues for small moduli of Na in more detail revealing that the parity symmetry broken states coalesce with the symmetric solution at $Na \approx -0.0075$ and with the antisymmetric solution at $Na \approx 0.0075$. In the region $|Na| \lesssim 0.0075$ the parity symmetry breaking solutions do not exist. The existence of these solutions is known as macroscopic quantum self-trapping [34].

B. Spectrum of the \mathcal{PT} -symmetric double well

Introducing the gain and loss contribution $\gamma = 0.02$ changes the eigenvalue spectrum significantly as can be seen in Fig. 1(b). The even and odd state with lower energies vanish and the two remaining states only exist for $Na \gtrsim -0.9$. These two states are \mathcal{PT} -symmetric, thus having a symmetric real part and an antisymmetric imaginary part (see Fig. 3(a),(b)). For the symmetry-breaking states the real part of the chemical potential is approximately identical to the case $\gamma = 0$ but the eigen-

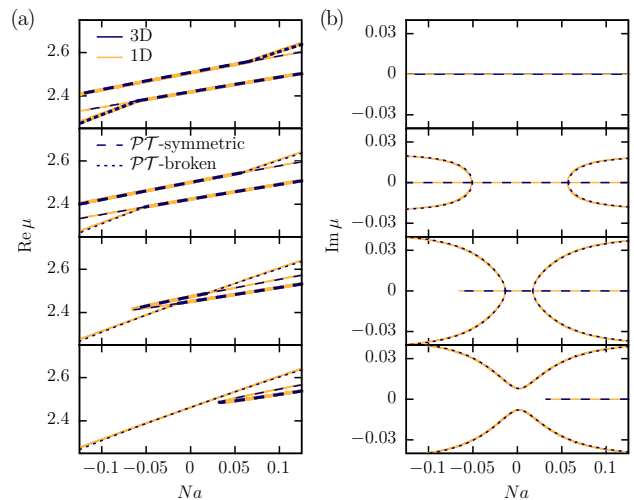


Figure 2. (Color online) (a) Real and (b) imaginary part of the chemical potential of the eigenstates for small values of Na . From top to bottom the four different gain/loss contributions $\gamma = 0, 0.02, 0.04$, and 0.042 are used. The eigenvalues of the \mathcal{PT} -symmetric and \mathcal{PT} -broken solutions in three dimensions are in excellent agreement with the numerically exact one-dimensional solutions. Stable branches are highlighted as thick lines (see Sec. III).

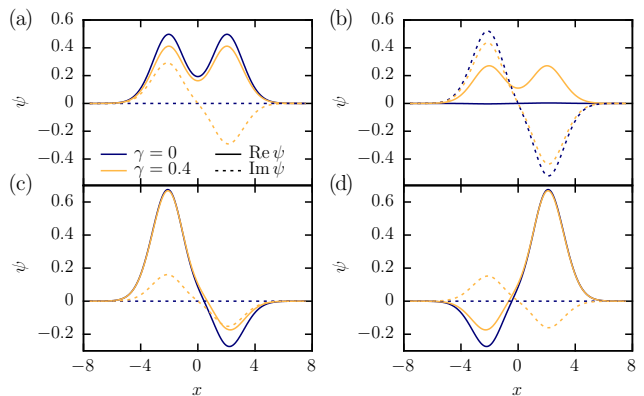


Figure 3. (Color online) Real (solid lines) and imaginary (dotted lines) part of the wave function of the \mathcal{PT} -symmetric ground (a) and first excited (b) state and the two \mathcal{PT} -broken states with a negative (c) and positive (d) imaginary part of the chemical potential. For $\gamma = 0$ the ground state is parity symmetric and the first excited state is antisymmetric. For finite values of γ the real part of both \mathcal{PT} -symmetric wave functions is even and the imaginary part is odd. The \mathcal{PT} -broken states are asymmetric thus breaking the \mathcal{PT} symmetry of the Hamiltonian.

value μ is now complex. Due to the \mathcal{PT} symmetry of the system, the two imaginary parts of μ have the same absolute value but different signs. The wave functions of the \mathcal{PT} -broken states are shown in Fig. 3(c),(d). To understand the behavior of the two tangent bifurcations of the symmetric and antisymmetric states we compare the

vicinity of the bifurcation points for $\gamma = 0$ and $\gamma = 10^{-3}$. Figure 1(c) shows that the two bifurcations vanish and a new tangent bifurcation between the two \mathcal{PT} -symmetric states arises.

If we want to compare the eigenvalues of the two \mathcal{PT} -symmetric states for different values of γ we have to choose a slightly different presentation since the difference between the eigenvalues of the two \mathcal{PT} -symmetric states is very small compared to their absolute change. Figure 1(d) shows $\mu - \bar{\mu}$ of the two \mathcal{PT} -symmetric states, where $\bar{\mu}$ denotes the mean value of μ of these two states. We immediately see that the tangent bifurcation at which the two \mathcal{PT} -symmetric states coalesce is shifted to greater values Na if the gain/loss parameter γ is increased. For $\gamma \gtrsim 0.41$ the bifurcation point is shifted to positive values of Na , i.e. the two \mathcal{PT} -symmetric solutions investigated here only exist for repulsive interaction of the atoms. At $Na \approx -0.8$ the chemical potential of the two \mathcal{PT} -symmetric states becomes equal for all parameters γ for which the \mathcal{PT} -symmetric states exist at $Na \approx -0.8$. However, at this point only a generic degeneracy of the energy eigenvalue μ occurs, the states themselves are different.

The relevant \mathcal{PT} -symmetric effects of the system, namely the breaking of \mathcal{PT} -symmetry, occur already at small absolute values of Na . This regime is shown in Fig. 2. The \mathcal{PT} -broken states emerge from the \mathcal{PT} -symmetric state in a pitchfork bifurcation. For an attractive interaction the \mathcal{PT} -broken solutions emerge from the \mathcal{PT} -symmetric ground state whereas in the case of repulsive interaction the \mathcal{PT} -broken branches emerge from the excited \mathcal{PT} -symmetric state (cf. middle two panels in Fig. 2). The \mathcal{PT} -broken solutions arise at approximately the same absolute value of Na for both attractive and repulsive interaction. As is known from \mathcal{PT} -symmetric systems the eigenvalues of the \mathcal{PT} -broken solutions occur in complex conjugate pairs. For increasing values of the gain/loss parameter γ the tangent bifurcation in which the two \mathcal{PT} -symmetric states vanish is shifted to greater values of Na . At the same time the \mathcal{PT} -broken solutions emerge already at smaller absolute values of Na . At strong enough values of γ the tangent bifurcation is shifted to repulsive interactions $Na > 0$ and the \mathcal{PT} -broken states exist even for $Na = 0$.

Although being solutions of the time-independent GPE the \mathcal{PT} -broken states are no stationary solutions of the time-dependent GPE. They experience an exponential gain or decay of the norm, thus effectively changing the nonlinearity parameter Na .

In the following we will restrict the discussion to small moduli of Na . As already mentioned in this regime the GPE is in good approximation solved by a product ansatz, thus reducing the problem to one dimension. The comparison in Fig. 2 confirms the excellent agreement between the calculations in one and three dimensions for the parameter range considered and justifies the reduction to one dimension used in the following sections. The solutions for the one-dimensional system (4) are obtained

with numerically exact methods by integrating the GPE outwards and fulfilling boundary conditions [26].

III. STABILITY

The first step towards understanding the dynamical properties of the system is the stability analysis of the stationary solutions with respect to small perturbations. The stability of the \mathcal{PT} -symmetric stationary states has already been discussed rudimentarily in [26]. We will shortly review these results and then focus on the stability in the vicinity of the bifurcations and the study of the dynamics of \mathcal{PT} -broken solutions.

In addition to the stability analysis in one dimension, which is presented in this section, we investigated the stability in three dimensions by linearizing the equations of motion of the time-dependent variational principle as described in [26]. In three dimensions excitations in y and z direction may give rise to additional instabilities. However, we found that in the parameter range considered these instabilities do not occur for $\omega_{y,z} \gtrsim 3$ and we again observe an excellent agreement between the calculations in one and three dimensions.

The time-dependent GPE is linearized in the vicinity of the stationary states, yielding the Bogoliubov-de Gennes equations

$$\Delta u = \left(V - \mu - \omega - 8N_0a |\psi_0|^2 \right) u - 4N_0a \psi_0^2 v, \quad (6a)$$

$$\Delta v = \left(V^* - \mu^* + \omega - 8N_0a |\psi_0|^2 \right) v - 4N_0a \psi_0^{*2} u. \quad (6b)$$

A solution of these equations determines the behavior of a perturbation $\delta\psi(x, t) = u(x) \exp(-i\omega t) + v^*(x) \exp(i\omega^* t)$ of a normalized stationary state at interaction strength N_0a . For real frequencies ω the perturbed state performs stable oscillations around the fixed point. If ω has a non-vanishing imaginary part it is necessary to distinguish between two cases. A negative imaginary part describes an exponentially damped and thus stable perturbation. By contrast, a perturbation increases exponentially if the imaginary part is positive. If one or more perturbations have a frequency with positive imaginary part the stationary solution is unstable otherwise it is stable. Due to the ansatz of the perturbation for every frequency ω with amplitudes (u, v) a second solution with frequency $-\omega^*$ and amplitudes (v^*, u^*) exists. Therefore all frequencies occur in pairs with positive and negative values of $\text{Re}\omega$. Applying the \mathcal{PT} operator to the Bogoliubov-de Gennes equations shows that if the stationary state ψ_0 has a perturbation frequency ω then $\mathcal{PT}\psi_0$ has a perturbation frequency ω^* . Thus for \mathcal{PT} -symmetric eigenstates every frequency is always part of a set of four solutions with $\pm \text{Re}\omega \pm i \text{Im}\omega$. For \mathcal{PT} -broken eigenstates perturbations occur in pairs $\pm \text{Re}\omega + i \text{Im}\omega$ and since \mathcal{PT} -broken solutions are mapped onto each other by application of the \mathcal{PT} operator their perturbation frequencies are complex conjugate.

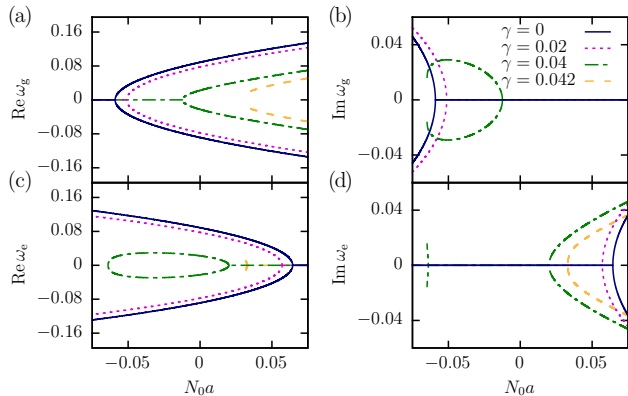


Figure 4. (Color online) (a),(c) Real and (b),(d) imaginary parts of the eigenvalues $\omega_{g/e}$ of the Bogoliubov-de Gennes equations for (a),(b) the ground state and (c),(d) the first excited state. Only the first nontrivial eigenvalue with smallest absolute real part is shown. Due to the symmetries of the equations the real and the imaginary parts of the eigenvalues both occur in pairs. Both states are stable for weak interactions but become unstable in the vicinity of the pitchfork bifurcations.

A. Stability of the \mathcal{PT} -symmetric solutions

The Bogoliubov-de Gennes equations are solved numerically exact by integrating the amplitudes u and v outwards and demanding that they vanish at the boundaries. The first nontrivial Bogoliubov-de Gennes eigenvalue with smallest absolute real part is shown in Fig. 4 for the two \mathcal{PT} -symmetric stationary states. Higher excitations are neglected since they have real eigenvalues thus describing stable perturbations.

For a weak gain/loss contribution $\gamma = 0.02$ the stability eigenvalues show that both \mathcal{PT} -symmetric stationary states are stable for small interaction strengths. The ground state (Fig. 4(a),(b)) becomes unstable at attractive interactions and the first excited state (Fig. 4(c),(d)) at repulsive interactions. Both stability changes occur near the pitchfork bifurcations at which the \mathcal{PT} -broken states emerge. For stronger gain/loss contributions $\gamma = 0.04$ the pitchfork bifurcations at which the two states become unstable are shifted to lower absolute values of $N_0 a$. Additionally we observe that the first excited state becomes unstable for attractive interactions shortly before it merges with the ground state at $N_0 a \approx -0.065$ in a tangent bifurcation and vanishes.

For gain/loss contributions $\gamma \gtrsim 0.41$ the \mathcal{PT} -broken states exist even for $N_0 a = 0$ and the \mathcal{PT} -symmetric stationary states exist only for repulsive interactions. In this case the ground state is stable for all interaction strengths whereas the excited state becomes unstable shortly after it emerges in the tangent bifurcation at $N_0 a \approx 0.03$. It is worth noting that the stability of the \mathcal{PT} -symmetric states changes not at the bifurcation points but only in their vicinity. The reason for this behavior is discussed

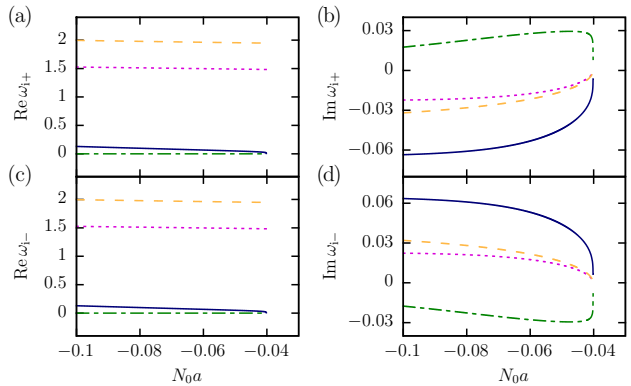


Figure 5. (Color online) (a),(c) Real and (b),(d) imaginary part of the Bogoliubov-de Gennes eigenvalues $\omega_{i\pm}$ for the \mathcal{PT} -broken states with (a),(b) positive and (c),(d) negative imaginary part of the chemical potential μ at $\gamma = 0.03$. The four eigenvalues with smallest real parts are shown. In addition to each eigenvalue ω a solution with negative real part $-\omega^*$ exists. All but one eigenvalue of the \mathcal{PT} -broken state with $\text{Im} \mu > 0$ ($\text{Im} \mu < 0$) have a negative (positive) imaginary part.

in detail at the end of this section.

B. Perturbations of the \mathcal{PT} -broken solutions

Although the \mathcal{PT} -broken solutions are no stationary solutions of the time-dependent GPE it is nevertheless instructive to solve the Bogoliubov-de Gennes equations for these states. We will see that this is relevant for the understanding of the dynamics of the condensate as well as the stability of the stationary \mathcal{PT} -symmetric solutions. Figure 5 shows the four Bogoliubov-de Gennes eigenvalues with smallest absolute real part for the two \mathcal{PT} -broken states using a constant value of the gain/loss parameter $\gamma = 0.03$. The stability eigenvalues of the \mathcal{PT} -broken state with $\text{Im} \mu > 0$ in Fig. 5(a),(b) show that the three eigenvalues with nonzero real part have a negative imaginary part. In fact there is an infinite number of further perturbations with negative imaginary part corresponding to higher excited states of the double well. There is, however, an additional solution with $\text{Re} \omega_{i+} = 0$ and a positive imaginary part describing a perturbation which increases exponentially. Since the \mathcal{PT} -broken solutions are not stationary the usual interpretation of the eigenvalues ω as stability indicators is invalid. The damped oscillatory behavior described by the eigenvalues with negative imaginary part and non-vanishing real part is characteristic for these states as will be seen in Sec. IV.

Since the \mathcal{PT} -broken states can be mapped onto each other by application of the \mathcal{PT} operator the \mathcal{PT} -broken state with $\text{Im} \mu < 0$ has the complex conjugate stability eigenvalues shown in Fig. 5(c),(d). This is a consequence

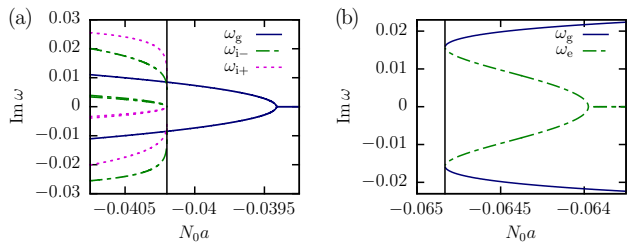


Figure 6. (Color online) Imaginary part of the Bogoliubov-de Gennes eigenvalues of all states involved in (a) the pitchfork bifurcation at $\gamma = 0.03$ and (b) the tangent bifurcation at $\gamma = 0.04$. The ground state becomes unstable before the pitchfork bifurcation at which the \mathcal{PT} -broken solutions arise. For decreasing $N_0 a$ the excited state becomes unstable before the tangent bifurcation at which the two \mathcal{PT} -symmetric states coalesce and vanish. At the bifurcations the stability eigenvalues of the states involved coalesce since the states themselves become equal. The bifurcation points are marked by black vertical lines.

of the fact that this state has the same dynamics as the \mathcal{PT} -broken state with $\text{Im} \mu > 0$ if evolved in negative time direction.

C. Stability at the bifurcation points

Both the ground state and the excited state become unstable near a bifurcation point. Therefore the Bogoliubov-de Gennes eigenvalues in the vicinity of the bifurcations are now investigated in more detail. Figure 6 shows the stability eigenvalues of all states involved in the bifurcations. It can immediately be seen that the stability properties of the \mathcal{PT} -symmetric states do not change at the bifurcation points but only in their vicinity. The ground state (Fig. 6(a)) is already unstable for greater values of $N_0 a$, i.e. the ground state becomes unstable in a parameter regime where the \mathcal{PT} -broken solutions do not yet exist. This was already found in a two-mode analysis of a \mathcal{PT} -symmetric double well [35]. A similar behavior is observed at the tangent bifurcation where the excited state becomes unstable shortly before the bifurcation point at which the \mathcal{PT} -symmetric solutions vanish (Fig. 6(b)).

This discrepancy is surprising because we know from real nonlinear systems that the stability of eigenstates changes at bifurcation points. Also in linear \mathcal{PT} -symmetric systems all eigenstates are stable unless a \mathcal{PT} -broken eigenstate with complex eigenvalue exists. In both cases a change in the stability of a stationary state coincides with a qualitative change in the spectrum.

As a first step we ensure that the investigation of the lowest-lying states is sufficient and higher excited states are not responsible for the discrepancy. Therefore we solved the Bogoliubov-de Gennes equations for the \mathcal{PT} -symmetric double-delta potential studied in [20, 36], a system in which only two \mathcal{PT} -symmetric and two \mathcal{PT} -

broken eigenstates exist. Indeed, also this system shows the discrepancy thus ruling out higher excited states as its origin [37]. It therefore seems likely that the observed discrepancy is a consequence of the combination that both a nonlinear and simultaneously \mathcal{PT} -symmetric system is investigated. Due to the non-Hermiticity the norm is not conserved thus the nonlinearity parameter $N a$ and consequently the spectrum changes with time. As a result the dynamical properties are not governed by the eigenvalue spectrum at a fixed interaction strength. Instead it is necessary to consider the whole spectrum as a function of $N a$, and thus the \mathcal{PT} -broken states are already dynamically accessible in the parameter regime where only \mathcal{PT} -symmetric states exist.

To confirm that this property is indeed the reason why the stability does not change at the bifurcation points we modify the Gross-Pitaevskii nonlinearity

$$|\psi(x, t)|^2 \rightarrow \frac{|\psi(x, t)|^2}{\int |\psi(x, t)|^2 dx}. \quad (7)$$

This formulation is equivalent to the mean-field limit of the \mathcal{PT} -symmetric Bose-Hubbard dimer by Graefe et al. in which such a discrepancy does not occur [38].

Replacing the nonlinearity with (7) does not change the normalized eigenstates of the GPE. It leads, however, to a different form of the Bogoliubov-de Gennes equations,

$$\begin{aligned} & \left(-\Delta + V - \omega - \mu - 8N_0 a |\psi_0|^2 \right) u - 4N_0 a v \psi_0^2 \\ & + 4N_0 a |\psi_0|^2 \psi_0 \int v \psi_0 + u \psi_0^* d^3 r = 0, \end{aligned} \quad (8a)$$

$$\begin{aligned} & \left(-\Delta + V^* + \omega - \mu^* - 8N_0 a |\psi_0|^2 \right) v - 4N_0 a u \psi_0^{*2} \\ & + 4N_0 a |\psi_0|^2 \psi_0^* \int v \psi_0 + u \psi_0^* d^3 r = 0. \end{aligned} \quad (8b)$$

These equations are solved in the vicinity of the bifurcations so that the results with the adapted nonlinearity (7) in Fig. 7 can directly be compared to the stability eigenvalues obtained with the usual Gross-Pitaevskii nonlinearity in Fig. 6. Using the adapted nonlinearity (7) the stability of the ground state changes at the bifurcation point, i.e. the ground state becomes unstable as soon as the \mathcal{PT} -broken solutions exist. Additionally the excited state does not show a stability change for attractive interaction but stays stable until it vanishes. Thus, the behavior observed that the stability of the \mathcal{PT} -symmetric states does not change at the bifurcation points but only in their vicinity is indeed a result of the norm-dependent nonlinearity of the GPE.

Also the behavior of the \mathcal{PT} -broken states does change by introducing the adapted nonlinearity. With the nonlinearity (7) the \mathcal{PT} -broken states are eigenstates of the time-dependent GPE with exponentially increasing or decreasing norm proportional to $\exp(2 \text{Im} \mu)$. Furthermore the \mathcal{PT} -broken states with positive and negative imaginary part are now a pure sink or source, respectively.

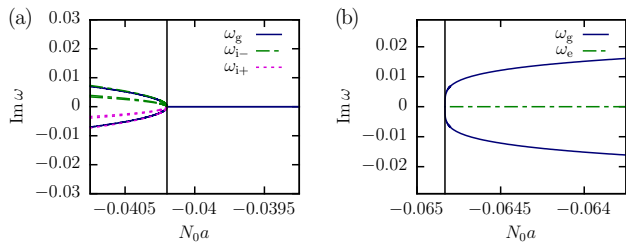


Figure 7. (Color online) Imaginary part of the stability eigenvalues ω of the Bogoliubov-de Gennes equations (8) for the norm-independent nonlinearity (7) in the vicinity of (a) the pitchfork bifurcation and (b) the tangent bifurcation. A constant gain/loss parameter (a) $\gamma = 0.03$ and (b) $\gamma = 0.04$ is used. The ground state becomes unstable at the pitchfork bifurcation and the excited state is stable until it vanishes at the tangent bifurcation. The \mathcal{PT} -broken states are now a pure sink or source. The bifurcation points are marked by black vertical lines.

IV. WAVE PACKET DYNAMICS

The linear stability analysis in the previous section describes the dynamical behavior in the vicinity of the eigenstates, and in the case of the \mathcal{PT} -broken solutions for very short time spans after which the spectrum changes. For finite time spans this is not sufficient. To gain a more elaborate picture of the dynamics the time evolution of wave packets is investigated for different values of the gain/loss parameter γ and the nonlinearity parameter Na .

We use the *split-operator method* to numerically calculate the time evolution of wave packets which is known to produce accurate results even for nonlinear equations as the GPE [39–41].

The oscillation of a single wave packet between the wells of the \mathcal{PT} -symmetric double-well potential has already been discussed in [26]. There the square modulus of the wave packets was investigated to analyze the characteristic phase shift of the oscillations. However, this representation does not allow for predictions of the behavior of arbitrary wave packets and the impact of the eigenstates of the system. We will now choose the Bloch sphere formalism as a different approach to visualize the time evolution of arbitrary states.

Even though Bloch sphere representations have already been used for \mathcal{PT} -symmetric [38, 42] as well as dissipative [5] two-mode BECs these studies always restricted the dynamics to the surface of the Bloch sphere. In non-Hermitian nonlinear systems, in which the norm is not conserved and the associated differential equation depends explicitly on the norm of the wave function, the dynamics is in general not restricted to this surface. We will see that the Bloch sphere provides a significant insight into the dynamical properties nonetheless.

A. Bloch sphere formalism

In general the representation as a Bloch sphere is limited to two-level quantum systems. Since the Hilbert space of the system investigated is not two-dimensional we use a projection to the space spanned by the \mathcal{PT} -symmetric ground state ψ_g and excited state ψ_e . In the linear case $Na = 0$ the time evolution of initial wave functions consisting of a linear superposition of the ground and excited state is restricted to this two-dimensional space. With interaction $Na \neq 0$ this is no longer true, however, our calculations show that for all time evolutions considered the projection to two dimensions is still a very good approximation.

We now choose two orthogonal basis vectors of the space spanned by the two \mathcal{PT} -symmetric stationary solutions. The first basis vector is identical to the normalized ground state $|e_1\rangle = |\psi_g\rangle$, and the second basis vector, $|e_2\rangle = \alpha(|\psi_e\rangle - \langle\psi_g|\psi_e\rangle|\psi_g\rangle)$ with normalization constant α , is the component of the excited state $|\psi_e\rangle$ orthogonal to $|e_1\rangle$ and is selected by application of the Gram-Schmidt method. Both basis vectors are exactly \mathcal{PT} -symmetric. An arbitrary wave function can be written as

$$|\psi\rangle = c_1 |e_1\rangle + c_2 |e_2\rangle + |\psi_{\text{err}}\rangle \quad (9)$$

with $c_1 = \langle e_1|\psi\rangle$ and $c_2 = \langle e_2|\psi\rangle$. Although all initial wave packets considered are superpositions of $|e_1\rangle$ and $|e_2\rangle$ the time evolution will in general leave the space spanned by $|e_1\rangle$ and $|e_2\rangle$. The norm of $|\psi_{\text{err}}\rangle$ measures the error made by the projection to the two-dimensional Hilbert space. In all calculations presented $\langle\psi_{\text{err}}|\psi_{\text{err}}\rangle < 0.004$ was found, justifying the projection.

The basis vectors $|e_1\rangle$ and $|e_2\rangle$ are defined to correspond to the north and south pole of the Bloch sphere, respectively, by introducing the spherical coordinates $R \in [0, \infty)$, $\varphi \in (-\pi, \pi]$ and $\vartheta \in [0, \pi]$ as follows

$$c_1 = R e^{i\chi+i\varphi} \cos(\vartheta/2), \quad (10a)$$

$$c_2 = R e^{i\chi} \sin(\vartheta/2), \quad (10b)$$

with an arbitrary phase $\chi \in \mathbb{R}$. Since $\langle\psi_{\text{err}}|\psi_{\text{err}}\rangle \ll 1$ the radius can be identified with the norm of the wave packet $R \approx \|\psi\|$. The orientation of the basis vectors on the Bloch sphere and the stationary solutions at a fixed value of γ are shown in Fig. 8.

The \mathcal{PT} symmetry of the system has several implications for the representation as a Bloch sphere. Since the system considered is non-Hermitian the norm of a wave packet is not conserved. The norm was identified with the radius R , thus in general the time evolution of an arbitrary wave packet is not constrained to the surface of the Bloch sphere but it will either dive into the sphere or leave the surface to larger radii. The two basis vectors are exactly \mathcal{PT} -symmetric thus application of the \mathcal{PT} operator leads to a complex conjugation of the coefficients c_1 and c_2 which is equivalent to the reflection

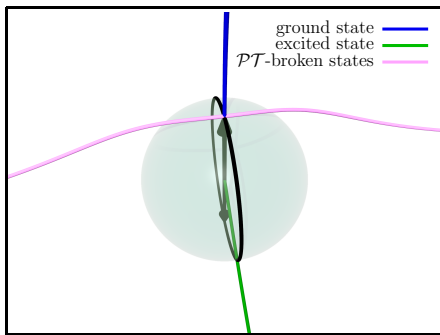


Figure 8. (Color online) The Bloch sphere representation using the coordinates defined in Eq. (10). The basis vectors $|e_1\rangle$ and $|e_2\rangle$ correspond to the north and south pole, respectively. On the front side of the plotted great cycle (black line) the azimuth angle is $\varphi = 0$ and on the back side $\varphi = \pi$. All states residing on the plane in which this great cycle lies are \mathcal{PT} -symmetric and the time evolution in the system is symmetric with respect to this plane. Furthermore the great cycle is used as the starting point for trajectories discussed in Sec. IV C. Additionally the four eigenstates are plotted for $\gamma = 0.03$ and the value of Na corresponding to the current location (cf. Sec. IV B).

$\varphi \rightarrow -\varphi$. Consequently all \mathcal{PT} -symmetric states reside on the plane defined by $\varphi \in \{0, \pi\}$.

A further implication of the \mathcal{PT} symmetry of the system is that if $\psi(x, t)$ is a solution of the time-dependent GPE then $\psi^*(-x, -t)$ is also a solution. Since \mathcal{P} reflects the spatial coordinate and \mathcal{T} applies only a complex conjugation $\psi^*(-x, -t) = \mathcal{PT}\psi(x, -t)$ holds and hence all trajectories are symmetric with respect to the plane $\varphi \in \{0, \pi\}$, in which the \mathcal{PT} symmetric eigenstates are found.

B. Eigenstates in Bloch sphere representation

Figure 9 shows both the eigenstates and time-evolved wave packets in the Bloch sphere representation. In this example the Bloch sphere represents the interaction strength $Na = N_0a = -0.05$. Since a larger radius is equivalent to a greater amount of particles, $N = N_0\|\psi\|^2 = N_0R^2$, plotting the \mathcal{PT} -symmetric and \mathcal{PT} -broken solutions of the time-independent GPE is another way of showing these eigenstates in dependence of Na . They are depicted as thick pink lines in Fig. 9 and can be seen most clearly in Fig. 9(a). Only attractive interactions are shown thus larger radii relate to more negative values of Na .

Both \mathcal{PT} -symmetric solutions start at the center of the sphere. The ground state goes through the north pole and the excited state goes through the south pole for $\gamma = 0$ (Fig. 9(a)). Increasing γ the penetration point of the excited state through the Bloch sphere wanders on the meridian $\varphi = 0$ to the north pole at which the ground state resides (cf. Figs 9(b)-(e)). For a critical value of γ

this point reaches the north pole, which is almost fulfilled in Fig. 9(f). For greater values of γ the \mathcal{PT} -symmetric solutions even vanish on the surface of the Bloch sphere and only exist within the sphere. This behavior of the stationary solutions on the surface of the Bloch sphere can be comprehended by comparison with the eigenvalue spectrum in Fig. 2 for different values of γ and a fixed value of Na .

As already shown in the eigenvalue spectrum the bifurcation at which the ground and excited state coalesce can also be reached by tuning Na . This can be seen in Fig. 9(e) where the two \mathcal{PT} -symmetric states coalesce at a critical radius outside the Bloch sphere resulting in the closed circle of the thick pink lines. For smaller values of γ shown in Fig. 9(a)-(d) the bifurcation point lies at a larger radius outside the figure.

Since attractive interactions are shown the two \mathcal{PT} -broken solutions emerge from the ground state. For the chosen interaction strength on the Bloch sphere $Na = -0.05$ the \mathcal{PT} -broken solutions emerge outside the sphere for $\gamma \gtrsim 0.022$ and inside the sphere for $\gamma \lesssim 0.022$. The \mathcal{PT} -broken solution with $\text{Im } \mu > 0$ ($\text{Im } \mu < 0$) lies on the left (right) side of the symmetry plane.

C. Dynamics on the Bloch sphere

After this short discussion of the eigenstates we now address the time evolution. For all calculations shown in Fig. 9 the initial wave packets are normalized and a linear superposition of $|e_1\rangle$ and $|e_2\rangle$, thus $R = 1$ and $\langle \psi_{\text{err}} | \psi_{\text{err}} \rangle = 0$. The azimuth angle is either $\varphi = 0$ or π , therefore all initial wave packets start on a great circle of the Bloch sphere through the north pole, south pole, and the excited stationary state. They are integrated in positive and negative time direction.

For the case $\gamma = 0$ shown in Fig. 9(a) the norm and therefore the radius are conserved quantities. All trajectories stay on the surface of the Bloch sphere. Both the stationary ground and excited state are elliptic fixed points and therefore stable.

This behavior changes drastically if a small gain/loss parameter $\gamma = 0.0025$ is introduced as done in Fig. 9(b). Due to the gain and loss, the norm of the wave packets are no longer conserved and the trajectories no longer run on the surface of the Bloch sphere. We identify two different regions on the great circle for initial wave packets which are delimited by the ground state, viz. the north pole, and the excited state. All wave packet starting in the region on the front side between the two fixed points (thick blue lines) evolve to a smaller norm inside the Bloch sphere whereas wave packets starting on the second region on the back side (red lines) evolve to a higher norm outside the sphere. The two \mathcal{PT} -symmetric stationary states are again elliptic fixed points, thus being stable. The sum of all oscillating trajectories of the wave packets define closed surfaces which cannot be penetrated by other trajectories.

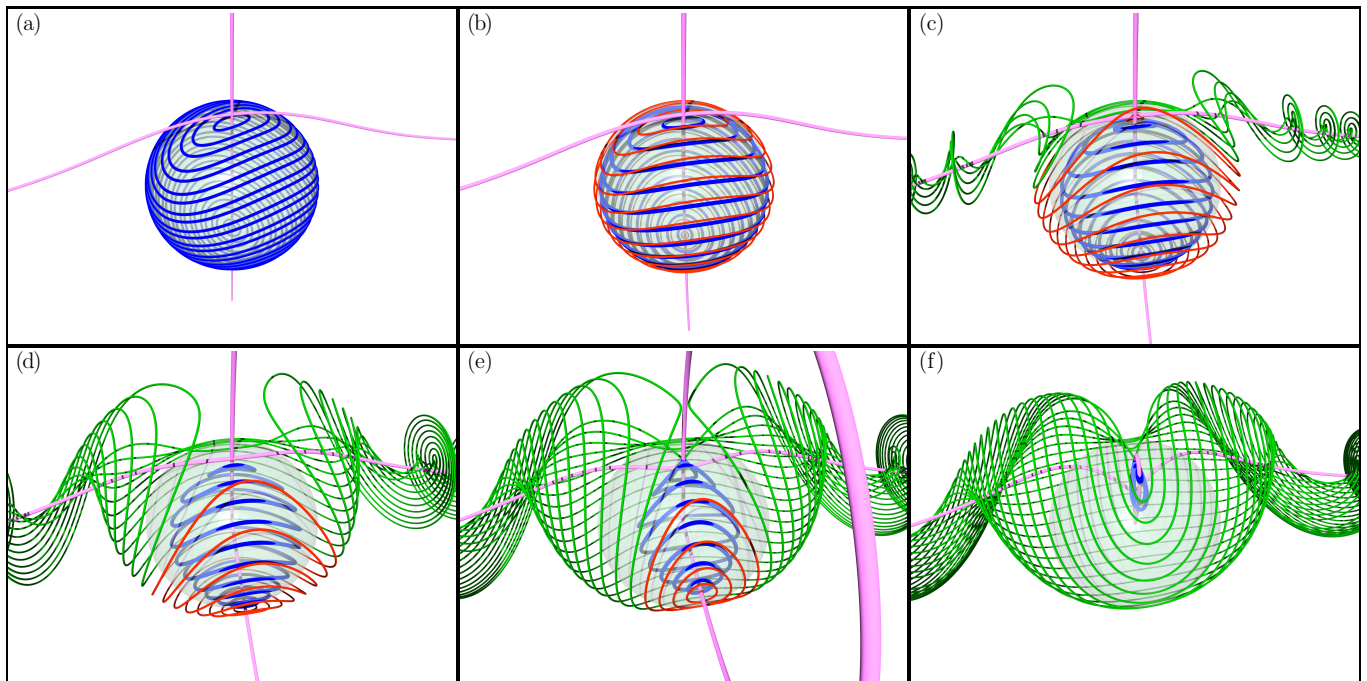


Figure 9. (Color online) The dynamics of wave packets projected to the space spanned by the \mathcal{PT} -symmetric ground and excited state illustrated on a Bloch sphere. The interaction strength $Na = -0.05$ on the surface of the sphere is constant in all figures whereas the gain/loss parameters are varied, with (a) $\gamma = 0$, (b) $\gamma = 0.0025$, (c) $\gamma = 0.01$, (d) $\gamma = 0.02$, (e) $\gamma = 0.03$, and (f) $\gamma = 0.04$. The solutions of the time-independent GPE are plotted for orientation (pink lines cf. Fig. 8). The ground state starts in the center of the sphere and goes through the north pole whereas the penetration point of the excited state is at the south pole for $\gamma = 0$ and wanders on the meridian $\varphi = 0$ to the north pole for increasing values of γ . The \mathcal{PT} -broken solutions emerge from the ground state. All wave packets shown start on a great cycle through the north pole, south pole and the excited state. Wave packets starting on the front side of the sphere evolve to a smaller norm thus diving into the sphere (closed thick blue lines inside the sphere). Wave packets starting in the remaining region of the great circle either show oscillations with a larger norm outside the sphere (closed red lines outside the sphere) or diverge while encircling the \mathcal{PT} -broken solutions (green lines departing from the left and the right side).

Increasing the gain/loss parameter to $\gamma = 0.01$ leads to the situation shown in Fig. 9(c). Again the wave packets starting on the front region between the two fixed points oscillate to a smaller norm and define a closed surface inside the Bloch sphere. However, the wave packets starting on the back region and oscillating outside the Bloch sphere do no longer define a closed surface. Instead an additional type of trajectories with diverging norm encircling the \mathcal{PT} -broken eigenstates appears. For $\gamma = 0.02$ the amount of diverging trajectories increases as can be seen in Fig. 9(d). These trajectories arrive from the vicinity of the \mathcal{PT} -broken state with $\text{Im}\mu < 0$ on the right side, touch the sphere, and leave the region of the sphere to larger radii R encircling the path of the \mathcal{PT} -broken state with $\text{Im}\mu > 0$ on the left side. This illustrates the role of the \mathcal{PT} -broken solutions for the dynamics of the condensate as sink and source.

Another qualitative change in the dynamical behavior is found for $\gamma = 0.03$ in Fig. 9(e). In agreement with the investigation of the linear stability in Fig. 4 the ground state is unstable for $Na = -0.05$, viz. exactly on the surface of the Bloch sphere. For lower values of γ there

is a region around the ground state in which only stable oscillations originate. For $\gamma = 0.03$ the ground state is unstable and all wave packets starting on the $\varphi = \pi$ meridian behind the ground state are diverging. Wave packets starting before the ground state still show stable oscillations evolving inside the sphere.

Finally for $\gamma = 0.04$ shown in Fig. 9(f) the two \mathcal{PT} -symmetric stationary solutions are almost identical and most wave packets starting on the great circle on the Bloch sphere diverge. Only wave packets starting in a small region around the stable excited state and in the region between the two stationary states still show stable oscillations. For even greater values of γ the stationary solutions do no longer exist on the surface of the Bloch sphere and no stable oscillations starting on the great circle can be observed.

V. CONCLUSION AND OUTLOOK

We studied the implications of \mathcal{PT} symmetry on the dynamical behavior and stability of a BEC with contact

interaction in a double-well potential.

Solving the Bogoliubov-de Gennes equations for non-Hermitian systems showed that the two \mathcal{PT} -symmetric stationary solutions with smallest chemical potential are stable as long as the \mathcal{PT} -broken states do not exist. However, the ground state becomes dynamically unstable in the vicinity of the pitchfork bifurcation at which the \mathcal{PT} -broken states emerge from the ground state at an attractive interaction strength. Analogously the excited state becomes unstable at repulsive interactions in the vicinity of the pitchfork bifurcation. The discrepancy between the bifurcations and the points at which the stability changes could be traced back to the norm dependency of the Gross-Pitaevskii nonlinearity.

Due to the non-Hermiticity of the system the dynamics is not governed by isolated fixed points but an infinite number of eigenstates which solve the time-independent GPE for the varying number of particles. The dynamics of the condensate was visualized using the Bloch sphere formalism although the dynamics is not constrained to the surface of the sphere due to the nonlinearity and non-Hermiticity of the system. Applying a small gain and loss of particles leaves the typical dynamics in a real double-well potential mostly intact but the trajectories now run slightly above or below the surface of the sphere describing a condensate with more or less particles, respectively.

For stronger gain/loss contributions an additional type of trajectories arises which describes a condensate localized in one well with a diverging number of particles. These diverging trajectories encircle the \mathcal{PT} -broken eigenstates of the time-independent GPE. However it is still possible to choose initial wave packets that show stable oscillations. In fact we observed that all \mathcal{PT} -symmetric wave functions which initially dive into the sphere always show stable oscillations. If the gain and loss is further increased most wave packets diverge and stable oscillations are only found in a small region in the vicinity of the excited state.

Understanding the dynamics of a BEC in a \mathcal{PT} -symmetric double well is the first step towards an experimental realization of a \mathcal{PT} -symmetric quantum system and the starting point for studies in more complex potentials and with additional interaction types like the dipolar interaction. Additionally it would be highly desirable to obtain a microscopic description of the in- and outcoupling process represented by an imaginary potential in the mean-field limit. Analyzing the bifurcation scenario at strong attractive interaction strengths switching from two tangent bifurcations to one in the presence of gain and loss as visible in Fig. 1 is an interesting task for future work from a more theoretical point of view and can probably be achieved using the analytic continuation described in [27].

-
- [1] N. Moiseyev, *Non-Hermitian Quantum Mechanics* (Cambridge University Press, Cambridge, 2011).
- [2] Y. Kagan, A. E. Muryshev, and G. V. Shlyapnikov, *Phys. Rev. Lett.* **81**, 933 (1998).
- [3] F. K. Abdullaev, V. V. Konotop, M. Salerno, and A. V. Yulin, *Phys. Rev. E* **82**, 056606 (2010).
- [4] Y. V. Bludov and V. V. Konotop, *Phys. Rev. A* **81**, 013625 (2010).
- [5] F. Trimborn, D. Witthaut, and S. Wimberger, *J. Phys. B* **41**, 171001 (2008).
- [6] D. Witthaut, F. Trimborn, H. Hennig, G. Kordas, T. Geisel, and S. Wimberger, *Phys. Rev. A* **83**, 063608 (2011).
- [7] J. R. Anglin and A. Vardi, *Phys. Rev. A* **64**, 013605 (2001).
- [8] A. Vardi and J. R. Anglin, *Phys. Rev. Lett.* **86**, 568 (2001).
- [9] T. Gericke, P. Wurtz, D. Reitz, T. Langen, and H. Ott, *Nat. Phys.* **4**, 949 (2008).
- [10] N. P. Robins, C. Figl, M. Jeppesen, G. R. Dennis, and J. D. Close, *Nat. Phys.* **4**, 731 (2008).
- [11] C. M. Bender and S. Boettcher, *Phys. Rev. Lett.* **80**, 5243 (1998).
- [12] C. M. Bender, S. Boettcher, and P. N. Meisinger, *J. Math. Phys.* **40**, 2201 (1999).
- [13] C. M. Bender, *Rep. Prog. Phys.* **70**, 947 (2007).
- [14] A. Mostafazadeh, *J. Math. Phys.* **43**, 205 (2002).
- [15] A. Mostafazadeh, *J. Math. Phys.* **43**, 2814 (2002).
- [16] A. Mostafazadeh, *J. Math. Phys.* **43**, 3944 (2002).
- [17] S. Klaiman, U. Günther, and N. Moiseyev, *Phys. Rev. Lett.* **101**, 080402 (2008).
- [18] J. Schindler, A. Li, M. C. Zheng, F. M. Ellis, and T. Kottos, *Phys. Rev. A* **84**, 040101 (2011).
- [19] S. Bittner, B. Dietz, U. Günther, H. L. Harney, M. Miski-Oglu, A. Richter, and F. Schäfer, *Phys. Rev. Lett.* **108**, 024101 (2012).
- [20] H. Cartarius and G. Wunner, *Phys. Rev. A* **86**, 013612 (2012).
- [21] T. Mayteevarunyoo, B. A. Malomed, and A. Reksabutr, *Phys. Rev. E* **88**, 022919 (2013).
- [22] E.-M. Graefe, *J. Phys. A* **45**, 444015 (2012).
- [23] C. E. Rüter, K. G. Makris, R. El-Ganainy, D. N. Christodoulides, M. Segev, and D. Kip, *Nat. Phys.* **6**, 192 (2010).
- [24] A. Guo, G. J. Salamo, D. Duchesne, R. Morandotti, M. Volatier-Ravat, V. Aimez, G. A. Siviloglou, and D. N. Christodoulides, *Phys. Rev. Lett.* **103**, 093902 (2009).
- [25] M. Kreibich, J. Main, H. Cartarius, and G. Wunner, *Phys. Rev. A* **87**, 051601(R) (2013).
- [26] D. Dast, D. Haag, H. Cartarius, G. Wunner, R. Eichler, and J. Main, *Fortschr. Physik* **61**, 124 (2013).
- [27] D. Dast, D. Haag, H. Cartarius, J. Main, and G. Wunner, *J. Phys. A* **46**, 375301 (2013).
- [28] A. D. McLachlan, *Mol. Phys.* **8**, 39 (1964).
- [29] S. Rau, J. Main, P. Köberle, and G. Wunner, *Phys. Rev. A* **81**, 031605(R) (2010).
- [30] S. Rau, J. Main, and G. Wunner, *Phys. Rev. A* **82**, 023610 (2010).
- [31] S. Rau, J. Main, H. Cartarius, P. Köberle, and G. Wunner, *Phys. Rev. A* **82**, 023611 (2010).
- [32] A. Gammal, T. Frederico, and L. Tomio, *Phys. Rev. A* **64**, 055602 (2001).

- [33] E. A. Donley, N. R. Claussen, S. L. Cornish, J. L. Roberts, E. A. Cornell, and C. E. Wieman, *Nature* **412**, 295 (2001).
- [34] M. Albiez, R. Gati, J. Fölling, S. Hunsmann, M. Cristiani, and M. K. Oberthaler, *Phys. Rev. Lett.* **95**, 010402 (2005).
- [35] A. S. Rodrigues, K. Li, V. Achilleos, P. G. Kevrekidis, D. J. Frantzeskakis, and C. M. Bender, *Rom. Rep. Phys.* **65**, 5 (2013).
- [36] H. Cartarius, D. Haag, D. Dast, and G. Wunner, *J. Phys. A* **45**, 444008 (2012).
- [37] A. Löhle, H. Cartarius, D. Haag, D. Dast, J. Main, and G. Wunner, “Stability of Bose-Einstein condensates in a \mathcal{PT} symmetric double- δ potential close to branch points,” (2014), arXiv:1401.2354 [quant-ph].
- [38] E. M. Graefe, H. J. Korsch, and A. E. Niederle, *Phys. Rev. A* **82**, 013629 (2010).
- [39] M. Feit, J. F. Jr., and A. Steiger, *J. Comput. Phys.* **47**, 412 (1982).
- [40] J. Fleck, J.A., J. Morris, and M. Feit, *Appl. Phys.* **10**, 129 (1976).
- [41] J. Javanainen and J. Ruostekoski, *J. Phys. A* **39**, L179 (2006).
- [42] E. M. Graefe, H. J. Korsch, and A. E. Niederle, *Phys. Rev. Lett.* **101**, 150408 (2008).